Phase transformation and light emission in Er-doped Si-rich HfO 2 films prepared by magnetron sputtering

Tetyana Torchynska, Brahim El Filali, Larysa Khomenkova, Xavier Portier, Fabrice Gourbilleau

Phase transformation and light emission in Er-doped Si-rich HfO_2 films prepared by magnetron sputtering

Tetyana Torchynska,[1,a)] Brahim El Filali,[2] Larysa Khomenkova,[3,4] Xavier Portier,[5] and Fabrice Gourbilleau[5]
[1]*Instituto Politécnico Nacional—ESFM, Av. IPN, México City 07738, Mexico*
[2]*Instituto Politécnico Nacional—UPIITA, Av. IPN, México City 07320, Mexico*
[3]*V. Lashkaryov Institute of Semiconductor Physics at NASU, 45 Pr. Nauky, Kyiv 03028, Ukraine*
[4]*Physics Department, National University "Kyiv-Mohyla Academy," 2 Skovorody str., Kyiv 04170, Ukraine*
[5]*CIMAP/UMR CNRS/CEA/ENSICAEN/UNICAEN, Bd. Marechal Juin, 4050 Caen Cedex 4, France*

(Received 9 December 2018; accepted 21 February 2019; published 11 March 2019)

The impact of phase transformation on the emission properties of Er-doped Si-rich HfO_2 films obtained by RF magnetron sputtering has been investigated by means of the scanning electron microscopy, energy dispersive x-ray spectroscopy, x-ray diffraction, x-ray photoelectron spectroscopy, and photoluminescence techniques. It has been observed that thermal treatment of the films at 950 and 1100 °C governs a phase separation process. The formation of HfO_2 nanocrystals of the tetragonal phase together with the Si-quantum dots (QDs) occurs at 950 °C. Upon annealing at 1100 °C, the tetragonal SiO_2 and monoclinic HfO_2 nanocrystals appear. The appearance of bright emission in the visible-near-infrared spectral range, related to the optical transitions in the 4*f* intrashell energy levels of Er ions, has been detected. The investigation of the annealing effect on the luminescent properties has revealed that the enhancement of Er^{3+} emission occurs due to an effective energy transfer from Si-QDs toward the Er ions. The oxidation of Si-QDs at high temperature annealing (1100 °C) leads to a reduction in the intensity of the Er ion related emission. Since hafnia-based materials have high density and are very sensitive to high-energy excitation, the results offer multifunctional applications of doped hafnia films, such as the luminescent materials for traditional phosphors. *Published by the AVS.* https://doi.org/10.1116/1.5085143

I. INTRODUCTION

The great interest shown on hafnia-based materials can be attributed to their applications as alternative dielectrics to SiO_2 in the Si-based CMOS technology[1,2] or as silica-hafnia-based waveguides.[3,4] Meanwhile, HfO_2 is characterized by a wide bandgap (≈5.8 eV), high transparency in the ultraviolet-visible spectral ranges, and a high refractive index (2.0–2.1 at 1.95 eV), making this material a good and attractive candidate for future photonic and optoelectronic applications.[5–7]

Additionally, the HfO_2-based materials are characterized by a low phonon cut-off energy (∼about 780 cm^{-1}) that reduces the probability of nonradiative phonon assisted relaxation and is attractive for doping these materials with different elements. The photoluminescence (PL) in pure HfO_2 was detected in near ultraviolet (4.0–4.2 eV) and visible (2.5–3.5 eV) spectral ranges.[8,9] The ultraviolet emission was attributed to the self-trapped exciton, but it is almost decayable at room temperature. On the other hand, the visible emission was assigned to the recombination via the different types of oxygen vacancies with trapped electrons.[8,9]

Some papers were related to the emission study in the HfO_2 films doped with the rare-earth elements, such as Nd, Er, Pr, etc.[7,10–14] Among different rare-earth trivalent elements, the Er^{3+} ion is one of the most popular due to its radiative transitions in the green ($^4S_{3/2} \rightarrow {}^4I_{15/2}$) and infrared ($^4I_{13/2} \rightarrow {}^4I_{15/2}$) spectral ranges being extensively used as an eye-safe source in the atmosphere, laser radar, and medical and surgical applications ($^4I_{11/2} \rightarrow {}^4I_{13/2}$).[15,16] However, the number of papers related to the spectroscopic investigation of HfO_2;Er based materials is few.

Binary silica-hafnia systems are of great interest as well because they allow thermal variation of the optical and structural properties, separating the SiO_2 and HfO_2 phases, and exert to study an influence of the nearest coordination shells on the emission of embedded rare-earth ions.[17] It is worth noting that Si-rich HfO_2 materials are considered mainly for microelectronic applications and that only a few emission studies on Er-doped SiO_2-HfO_2 materials have been presented till date.[10,12] However, the mechanism of the Er^{3+} ion excitation has not been reported. Moreover, the phenomenon of any formation of the Si nanocrystals or Si quantum dots (QDs) in hafnia has also not been observed.

The fact that the first coordination shell around the Er^{3+} ions is composed of five to six oxygen atoms at a distance ≈2.32–2.35 Å was discovered early. However, in regard to the other coordination shells, the situation is not clear yet. It was shown that in a binary system, the Er^{3+} ions were mainly dispersed in an amorphous HfO_2 environment.[17] But the question of the interaction of rare-earth ions with host defects and the dependence of their emission on the crystal phase of the surrounding matrix has not been clarified yet. In the present paper, we focus on the study of the phase

Note: This paper is part of the Special Topic Collection on Complex Oxides.
a)Electronic mail: ttorch@esfm.ipn.mx

transformation in the Si-rich hafnia oxide system versus annealing temperatures and its impact on the emission via the Er^{3+} ion inner electronic shells.

II. EXPERIMENTAL SETUP

Er-doped Si-rich HfO_2 films were grown by RF magnetron sputtering. The deposition was performed on the 2-in. B-doped (100) oriented Si wafers with a resistivity of about 15 Ω cm. All substrates were submitted to standard RCA cleaning [dipped in a diluted hydrofluoric solution (10%) followed by cleaning in deionized water and drying in pure N_2 flow] prior to their transfer in a load-lock vacuum chamber of the deposition setup. A pure HfO_2 target (99.9%) topped with calibrated Si and Er_2O_3 pellets was used. The Si and Er_2O_3 pellets covered about 12% of the target surface each. The deposition was performed in a pure Ar plasma with an argon flow $f_{Ar} = 3$ sccm at a constant plasma pressure [$P = 0.039$ mbar (3.9 Pa)]. The RF power density and the substrate-cathode distance were 0.74 W/cm^2 and 57 mm, respectively. The temperature of the substrate was kept at 500 °C and the deposition time was 200 min. All the films were found to be homogeneous and uniform. The average thickness was about 800 nm.

After the deposition, each substrate was cut into a set of small pieces (usually 1×1 cm^2) to study the effect of the annealing treatment. It was performed in a conventional horizontal furnace at different temperatures in a continuous nitrogen flow [48 sccm with a pressure of about 1.4 mbar (140 Pa)]. Henceforth, the samples annealed at $T_A = 950$ and 1100 °C during $t_A = 15$ min will be discussed in detail.

Several experimental techniques were used to analyze the properties of the films. The PL emission was excited with a 325 nm line of a He-Cd laser and a 476 or 488 nm line of an Ar laser. PL spectra were recorded using several setups: (i) a Jobin Yvon TRIAX180 monochromator linked with a fast Hamamatsu photomultiplier and a Stanford Research Systems (SRS) lock-in amplifier (SP830 DPS) (for a 400–1000 nm spectral range) and (ii) a Jobin Yvon 1 m single grating monochromator coupled to a Northcoast Germanium detector cooled with liquid nitrogen and an SRS lock-in amplifier (SP830 DPS) (for an 800–1700 nm spectral range). The referenced chopping frequency was 20 Hz.

To study the surface morphology of the films, as well as to get information on their chemical composition, a scanning electronic microscope (SEM) Quanta 3D FEG-FEI with an additional detector Apollo X10 mark EDAX for energy dispersive x-ray spectroscopy (EDS) was used. X-ray diffraction (XRD) results were obtained using the equipment of Model X'PERT MRD with a Pixel detector, a three axis goniometry, and a parallel collimator with an angular resolution of 0.0001°. X-ray beam was achieved from the Cu source ($K_{\alpha 1}$ line, $\lambda = 1.5406$ Å).

To detect the film chemical composition, the x-ray photoelectron spectroscopy (XPS) was used that was realized in the Thermo Scientific™ K-Alpha™ XPS spectrometer. X-rays were obtained from the Al anode (K_a radiation with an energy of 1486.7 eV) operated at 15 kV (90 W) at a pressure of 1.33×10^{-7} Pa during the data collection. The 400 μm spot of the x-ray beam was set in two pass energy modes of 160 and 40 eV. To analyze the XPS spectra, the THERMO AVANTAGE V5.938 software was applied. All experiments were carried out at room temperature.

III. RESULTS AND DISCUSSION

A. EDS and SEM study

The surface morphology of as-grown and annealed samples was studied by the SEM method. As one can see from Fig. 1, the as-grown film has a smooth undeveloped

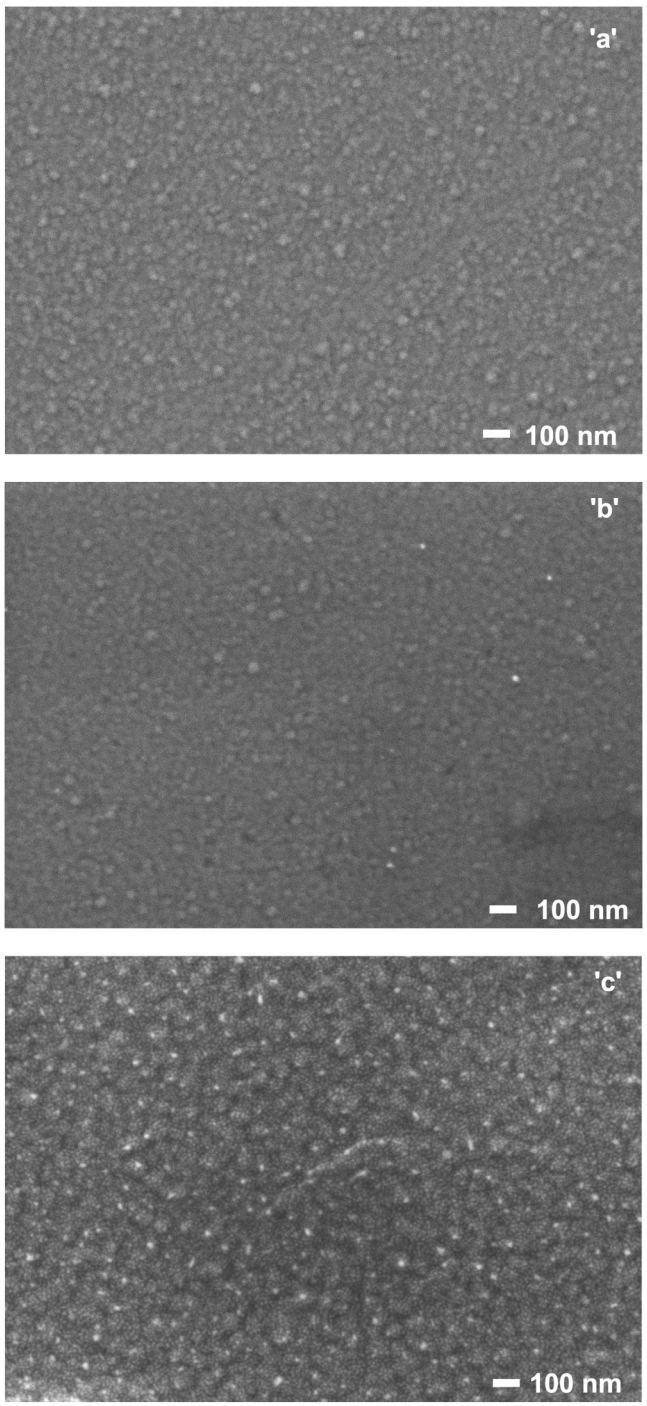

FIG. 1. SEM images of Si-HfO_2:Er films: as-grown (a) and after annealing at 950 °C (b) and 1100 °C (c).

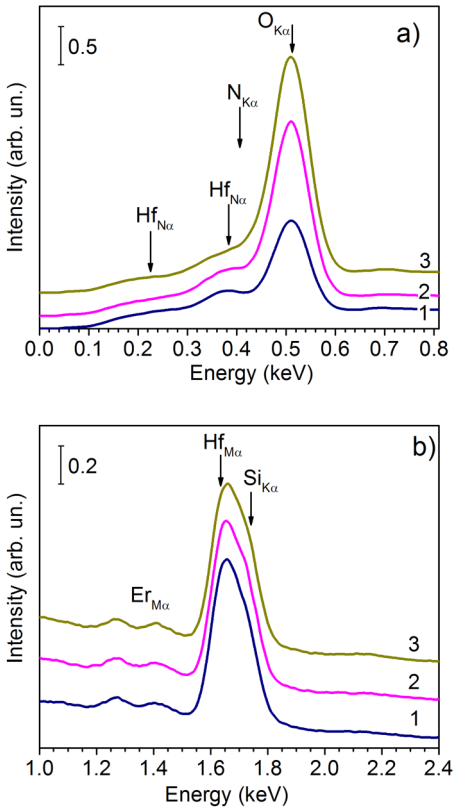

FIG. 2. EDS spectra recorded for the as-grown (1) and annealed at 950 °C (2) and 1100 °C (3) films. The energy ranges are 0–0.8 keV (a) and 1.0–2.4 keV (b).

surface [Fig. 1(a)]. Contrary to this, all annealed films demonstrate a developed structure, i.e., the grains form the microclusters separated by the valleys [Figs. 1(b) and 1(c)]. The sizes of the grains depend on the annealing temperature, i.e., for $T_A = 950$ °C, their mean size is in the range of 20–60 nm, while for $T_A = 1100$ °C, it is found to vary from 40 to 100 nm.

The EDS spectra for as-grown and annealed films are shown in Fig. 2. Hf, Si, O, N, and Er elements are found for all films [Figs. 2(a) and 2(b)]. The assignment of most pronounced peaks in the EDS spectra was performed taking into account atomic-binding energies for the elements of interest (Table I).

The annealing treatment results in the evolution of the shape of EDS spectra. It is at a significant range of E = 0.35–0.55 keV, i.e., the intensity of the $O_{K\alpha}$ signal (Fig. 2, curves 2 and 3) increases with annealing temperature enlargement (Table II). This can be caused by the adsorption of water-like entities from the atmosphere on the surface of as-grown films and oxygen penetration into the film depth during annealing. Besides, an appearance of nitrogen in the films after annealing (Table II) can also modify these spectra. The $N_{K\alpha}$ signal is observed usually at E = 0.398–0.402 keV and can be hardly distinguished due to its overlapping with the $Hf_{N\alpha}$ signal [Fig. 2(a)]. The enrichment of the films in oxygen and nitrogen can be explained taking into account the results of Ref. 18. It was reported that annealing at 1000 °C in a nitrogen atmosphere of HfSiON thin films causes the transport of O and N elements into the film depth.[18] Similar processes can occur in the studied films as well. It is noteworthy that

TABLE I. Atomic-electron binding energies (in keV) for the elements of interest (data extracted from the Table of Isotopes, CD-ROM Edition, Version 1.0, March 1996). The bold values correspond to arrays in Fig. 2.

	Element				
Atomic shell	7 N	8 O	14 Si	68 Er	72 Hf
K	**0.4016**	**0.5320**	**1.8389**	57.4855	65.3508
L_1	0.0244	0.0285	0.1487	9.7513	11.2707
L_2	0.0092	0.0071	0.0995	9.2643	10.7394
L_3	0.0092	0.0071	0.0989	8.3579	9.5607
M_1			0.0076	2.2065	2.6009
M_2			0.0030	2.0058	2.3654
M_3			0.0030	1.8118	2.1076
M_4				1.4533	**1.7164**
M_5				**1.4093**	1.6617
N_1				0.4491	0.5381
N_2				0.3662	0.4370
N_3				0.3200	**0.3804**
N_4				0.1767	**0.2238**
N_5				0.1676	0.2137

the intense $Si_{K\alpha}$ signal can be a superposition of the signal from the Si phase inside the film (if any) and that from the underlying substrate.

B. XRD study

XRD patterns recorded with the symmetric geometry are shown in Fig. 3. It is seen that the XRD pattern of the as-grown film has two broadbands centered at about 32.16° and 55.11° [Fig. 3(a)]. These two XRD bands can be attributed to the amorphous phase of the chemical composition $HfSiO_x$. Actually, these peaks were detected in the amorphous phase and then in the crystalline hafnium silicate of the tetragonal phase (ICSD Ref. code 00-036-0088) after annealing.[2,4,7]

Additionally, the XRD pattern presents a set of small intensity XRD peaks, i.e., at $2\Theta = 30.09°$ (a), 38.57°(b), 44.84° (c), 53.12° (d), 56.01° (e), 59.64° (f), 65.72° (g), 76.39° (h), and 78.96° (k) [Fig. 3(a)]. These peaks can originate from other phases that appeared due to the deposition of the films at 500 °C. It is possible that the crystallization process occurs at such temperature.

The XRD peaks at $2\Theta = 30.09°$ (a) and 59.64° (f) were identified as the XRD signals of the tetragonal HfO_2 phase (ICSD Ref. code 00-008-0342). The XRD peaks at $2\Theta = 56.01°$ (e) and 76.39° (k) can be attributed to the cubic Si phase (ICSD Ref. code 00-005-0565). The XRD peak at

TABLE II. Chemical film composition.

Samples element	As-deposited (%)	$T_A = 950$ °C (%)	$T_A = 1100$ °C (%)
O_K	49.5	60.3	66.2
Er_M	9.7	7.3	6.2
Hf_M	26.7	20.1	17.2
Si_K	12.6	9.5	8.1
N_K	1.5	2.8	2.3

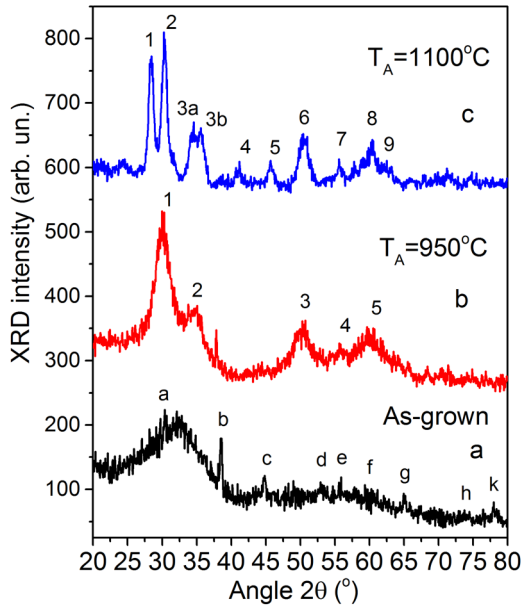

FIG. 3. XRD patterns of Si-HfO_2:Er films: as-grown (a) and annealed at 950 °C (b) and 1100 °C (c).

$2\Theta = 44.84°$ (c) can be assigned to the tetragonal $HfSiO_4$ crystal lattice (ICSD Ref. code 00-036-0088), whereas the XRD peaks at $2\Theta = 38.57°$(b), 53.12° (d), 65.72° (g), and 78.96° (k) were identified as the monoclinic $Er_2Si_2O_7$ crystal structure (ICSD Ref. code 01-072-0650).

The thermal treatment of the films at $T_A = 950$ °C led to changes in the XRD pattern. The signals from the tetragonal $HfSiO_4$ and monoclinic $Er_2Si_2O_7$ phases disappeared, while the XRD peaks owing to the tetragonal HfO_2 phase centered at $2\Theta = 30.09°$ (1), 35.09° (2), 49.55° (3), and 59.64° (5) increased significantly [Fig. 3(b)]. The XRD peak at $2\Theta = 56.01°$ (4) related to the cubic Si crystal lattice is still possible to detect in the XRD pattern [Fig. 3(b)].

Thermal treatment of the films at $T_A = 1100$ °C results in the further evolution of XRD patterns. The signals from the tetragonal HfO_2 phase have been not detected anymore. Instead the two sets of XRD peaks with significant intensities have appeared [Fig. 3(c)]. The first set of XRD peaks detected at $2\Theta = 28.38°$ (1), 34.55° (3a), 35.58° (3b), 41.17° (4), 50.38° (6), and 55.57° (7) has been assigned to the monoclinic HfO_2 phase (ICSD Ref. code 00-034-0104). The second set of XRD peaks detected at $2\Theta = 30.24°$ (2), 45.67° (5), 60.52° (8), and 62.97° (9) has been attributed to the tetragonal SiO_2 crystal structure (ICSD Ref. code 00-045-1374). Thus, annealing at $T_A = 1100$ °C stimulates the transformation of the tetragonal $HfSiO_4$ and HfO_2 crystal phases, detected in the as-grown samples, into the monoclinic HfO_2 phase. At the same time, the XRD signal from the Si phase decreases, which can be caused by the formation of the tetragonal SiO_2 phase.

The coherent domain sizes, d, were estimated for all investigated films from the half width of the most intensive peaks using Scherrer's formula.[19] It was found that in some as-grown films $d = 13.7$ Å, demonstrating the trend to increase up to $d = 29.4$ Å ($T_A = 950$ °C) and 82.5 Å ($T_A = 1100$ °C) in annealed films.

C. Light emitting study

PL spectra of the studied films are presented in Fig. 4 for the visible spectral range and in Fig. 5 for the infrared spectral range. The as-grown film demonstrates a weak visible PL emission with a maximum at about 2.78 eV under excitation by 325 nm light [Figs. 4(a) and 4(b)].

Annealing at $T_A = 950$ °C enhances the PL intensity significantly [Fig. 4(a)], whereas thermal treatment at $T_A = 1100$ °C enlarges it slightly [Fig. 4(b)]. It was reported recently[20] that for similar films, the brightest PL emission in the visible spectral range under 476-nm excitation was achieved upon annealing at $T_A = 900$–950 °C. It was ascribed to the formation of Si nanocrystals (Si-QDs) that, along with the defects of the matrix, significantly contribute to the visible emission. Taking into account those PL results, the detailed analysis of crystal phase transformation in the films annealed at 950 and 1100 °C is compared in the present paper.

It is clear that the PL spectrum of the film annealed at $T_A =$ 950 °C presents the superposition of four PL bands centered at 2.03, 2.40, 2.78, and 3.18 eV [Fig. 4(a)]. The comparison of PL properties of the pure and Si-rich HfO_2 films reported in Ref. 20 shows that the Si-incorporation into HfO_2 results in the

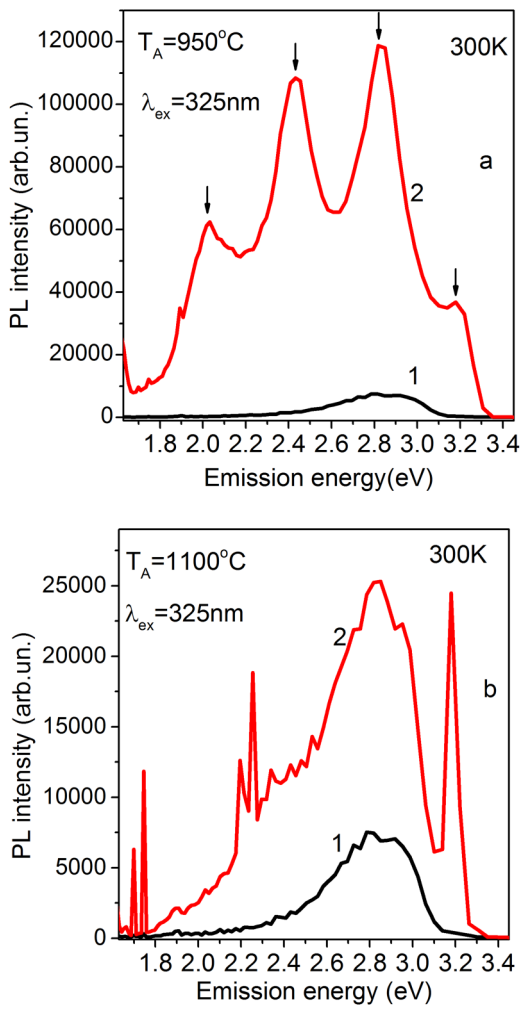

FIG. 4. Visible PL spectra of Si-HfO_2:Er films: as-grown (1a,1b) and annealed at 950 °C (2a) and 1100 °C (2b).

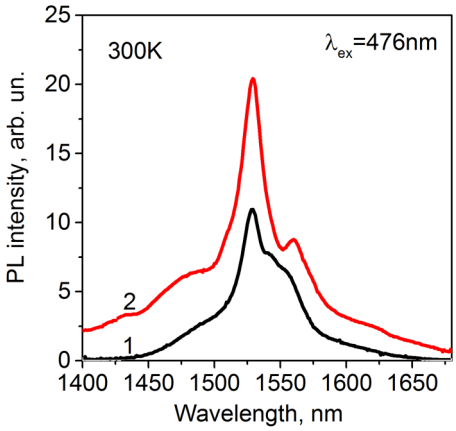

FIG. 5. Infrared PL spectra of the films annealed at 1100 °C (1) and 950 °C (2). Excitation light wavelength is 476 nm.

appearance of orange-red emission (2.03–2.13 eV) upon the annealing treatment. This PL band was found to be similar to that observed in the Si-rich SiO_2 materials[21,22] and was explained by the exciton emission in Si-quantum dots.[20] Note that XRD results presented above for similar Si-rich HfO_2 films confirmed the existence of Si inclusions in the tetragonal HfO_2 matrix. Thus, the PL band at 2.03 eV in studied films can be assigned to the exciton emission in Si-QDs.

The PL peak centered at 2.40 eV, which has been detected after annealing at 950 °C [Fig. 4(a)] and has not appeared after annealing at 1100 °C [Fig. 4(b)], can be assigned to the recombination via the different types of oxygen vacancies with trapped electrons in the films.[8,9] The additional oxidation of the films annealed at 1100 °C, that was confirmed by the EDS study (Fig. 2), reduces the amount of oxygen vacancies. As a result, the intensity of the PL band peaked at 2.40 eV decreases as well [Fig. 4(b)].

The formation of Si-QDs in the films mediates the excitation of rare-earth ions. It is known that the absorption cross section of rare-earth ions for 4*f*-4*f* transitions is about 10^{-19}–10^{-21} cm^{-2}, and these ions require a high power laser for their direct excitation.[23–28] The more promised transition is the 4*f*-5*d* ones with a larger absorption cross section (about 10^{-18} cm^{-2}). However, the excitation belongs to the ultraviolet spectral range, restricting its use for many applications.

It was reported that the host-mediated excitation of 4*f*-4*f* transitions can be very effective due to energy transfer. This approach was widely used for the rare-earth doped silica with embedded Si nanoclusters or QDs.[23–27] The Si-QD incorporation allowed increasing the absorption cross section of Er^{3+} ions from 10^{-21} cm^{-2} (Ref. 28) up to 10^{-16} cm^{-2}.[26,27] Simultaneously, the bright emission from Er^{3+} ions was achieved due to the effective energy transfer from Si-QDs into Er ions. For this purpose, the visible broadband excitation was used offering the safe applications of these materials. Thus, on the basis of the analogy with Si-QDs embedded in the SiO_2 host, one can suppose that an incorporation of Si-QDs in the hafnia oxide matrix can allow one to achieve an effective Er^{3+} ion excitation in the visible spectral range.

Thus, two PL bands centered at 2.78 and 3.18 eV [Fig. 4(a)], as well as the IR emission (Fig. 5) detected in the film annealed at 950 °C, have been attributed to the well-known optical transitions via the 4*f* intrashell energy levels in the Er^{3+} ions: $^4F_{3/2.5/2}$-$^4I_{15/2}$ at 455 nm (2.72 eV), $^4G_{11/2}$-$^4I_{15/2}$ at 400 nm (3.10 eV), and $^4I_{13/2}$-$^4I_{15/2}$ at 1.525–1.545 μm (0.803–0.813 eV).[29–31] Furthermore, the bright PL emission from the films annealed at 950 °C can be explained by the excitation energy transfer from the Si-QD, or native defects (V_O), toward the Er^{3+} ions, and/or by the reabsorption of Si-QD or native defect emissions by the Er^{3+} ion and its excitation via the up-conversion mechanism.[32]

TABLE III. Detected PL peaks and their legends.

Peak energy (eV)	Peak wavelength (nm)	Transition	Reference
1.698	730	$^4F_{11/2}$-$^4I_{15/2}$	30
1.746	710	$^4F_{9/2}$-$^4I_{15/2}$	30
2.194	565	$^4S_{5/2}$-$^4I_{15/2}$	30
2.254	550	$^4S_{3/2}$-$^4I_{15/2}$	30
2.339	530	$^2H_{11/2}$-$^4I_{15/2}$	30
2.530	490	$^4F_{7/2}$-$^4I_{15/2}$	31
2.720	455	$^4F_{5/2}$-$^4I_{15/2}$	31
2.850	435	$^4F_{3/2}$-$^4I_{15/2}$	30
2.952	420	$^2H_{9/2}$-$^4I_{15/2}$	30
3.178	390	$^4G_{11/2}$-$^4I_{15/2}$	30

The PL spectrum of the film annealed at $T_A = 1100$ °C has changed dramatically [Fig. 4(b)]. The PL intensities of all PL bands related to the optical transitions via the 4*f* intrashell energy levels in the Er ions have increased and the new PL bands appear. Note that the PL band (at 2.03 eV), related to the exciton emission in Si-QDs, and the PL band (at 2.40 eV) owing to the recombination via oxygen vacancies have been not detected in the PL spectrum. This correlates with the XRD results presented above, which show that the Si inclusions have not been detected in the films after the high temperature treatment (1100 °C).

PL peak positions of new PL bands and their legends are summarized in Table III. At high temperature, the process of phase transformation is realized efficiently, and two phases, the tetragonal SiO_2 and the monoclinic HfO_2, have been revealed in the XRD study. Earlier it was shown that in binary silica-hafnia systems, the Er^{3+} ions were located mainly in the hafnia oxide.[17] Thus, we can conclude that Er^{3+} ions in the Si-HfO_2:Er film after annealing at 1100 °C locate in the monoclinic HfO_2 phase mainly. Nevertheless, the different full widths at the half maximum of detected PL bands [Fig. 4(b)] testify that the Er ions (partially) exist in the second tetragonal SiO_2 phase as well.

D. XPS study

To confirm that the Si-QDs exist in the films after annealing at 950 °C and disappear after the temperature treatment at 1100 °C, the high resolution x-ray photoelectron spectra for the Si2p line were measured (Fig. 6). Two peaks centered at 98.48 and 101.48 eV have been detected in the XPS spectrum of as-grown films (Fig. 6, curve 1). These two peaks were assigned to x-ray photoelectron excitation

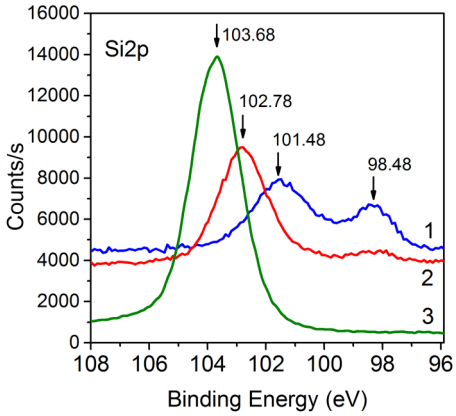

FIG. 6. XPS spectra obtained for the Si2p line in Si-HfO_2:Er films: as-grown (1) and annealed at 950 °C (2) and 1100 °C (3).

from the Si2p energy levels of Si atoms located in the monocrystalline Si (98.48 eV) and in the amorphous $HfSiO_x$ phase (101.48 eV).[33] Annealing at 950 °C triggers a partial decrease in the intensity of the Si2p peak related to the monocrystalline Si (98.48 eV) and the shift to 102.78 eV of the second Si2p peak connected with the Si atoms located in the Si suboxide. The latter process is attributed to the Si atoms in the tetragonal SiO_x crystal lattice. Annealing at 1100 °C leads to a total disappearence of the Si2p peak related to the monocrystalline Si (98.48 eV) and a significant increase of the Si2p peak at 103.68 eV owing to the Si atoms in the tetragonal SiO_2 crystal lattice.[33] Thus, at high annealing temperature, the Si atoms contribute to the formation of the tetragonal SiO_2 phase. One can conclude that the disappearence of Si-QD in the films at high annealing temperature (1100 °C) is the reason for the reduction in the PL intensity in comparison with that registered for the films annealed at 950 °C.

IV. SUMMARY AND CONCLUSIONS

In the present study, the impact of phase transformation on the emission properties of the Si-rich HfO_2:Er films obtained by RF magnetron sputtering was investigated by means of the SEM, EDS, XRD, XPS, and PL techniques. It was observed that the thermal treatment governs a phase separation process and the formation of (i) the small nanocrystals (≈2.9 nm) of tetragonal HfO_2 phase together with the inclusion of Si-QDs at 950 °C annealing and (ii) the larger nanocrystals (≈8.2 nm) of the tetragonal silica and monoclinic hafnia phases at 1100 °C annealing. Bright emission in the visible-near-infrared spectral range occurred. The investigation of the effect of annealing treatment on luminescent properties revealed that the enhancement of Er^{3+} emission occurs due to an effective energy transfer from Si-QDs, or naive defects, toward Er ions. The oxidation of Si-QDs at high temperature annealing (1100 °C) leads to a reduction of intensity in the Er ion related emission. Since hafnia-based materials have high density and are very sensitive to high-energy excitation, our results offer multifunctional applications of doped hafnia films, such as luminescent materials for traditional phosphors.

ACKNOWLEDGMENTS

This work was partly supported by the National Academy of Sciences of Ukraine (Project No. III-4-16), the Ministry of Education and Science (Project ID 89452), the Normandie Region and the European Regional Development Fund (ERDF) (Project LUMIERE), as well as by the CONACYT Mexico (Project No. 258224) and SIP-IPN Mexico (Project No. 20180495).

[1]G. He, L. Q. Zhu, Z. Q. Sun, Q. Wan, and L. D. Zhang, Prog. Mater. Sci. **56**, 475 (2011).
[2]L. Khomenkova, X. Portier, J. Cardin, and F. Gourbilleau, Nanotechnology **21**, 285707 (2010).
[3]R. R. Gonçalves *et al.*, Appl. Phys. Lett. **81**, 28 (2002).
[4]M. Mattarelli *et al.*, Opt. Mater. **31**, 1362 (2009).
[5]J. M. Khoshman, A. Khan, and M. E. Kordesch, Surf. Coat. Technol. **202**, 2500 (2008).
[6]O. Stenzel, S. Wilbrandt, S. Yulin, N. Kaiser, M. Held, A. Tünnermann, J. Biskupek, and U. Kaiser, Opt. Mater. Express **1**, 278 (2011).
[7]L. Khomenkovaa, Y.-T. An, D. Khomenkov, X. Portier, C. Labbé, and F. Gourbilleau, Physica B **453**, 100 (2014).
[8]M. Kirm, J. Aarik, M. Jürgens, and I. Sildos, Nucl. Instrum. Methods A **537**, 251 (2005).
[9]K. Smits, L. Grigorjeva, D. Millers, A. Sarakovskis, J. Grabis, and W. Lojkowski, J. Lumin. **131**, 2058 (2011).
[10]V. Kiisk, I. Sildos, S. Lange, V. Reedo, T. Tatte, M. Kirm, and J. Aarik, Appl. Surf. Sci. **247**, 412 (2005).
[11]L. X. Liu, Z. W. Ma, Y. Z. Xie, Y. R. Su, H. T. Zhao, M. Zhou, J. Y. Zhou, J. Li, and E. Q. Xie, J. Appl. Phys. **107**, 024309 (2010).
[12]G. C. Righini *et al.*, J. Non Cryst. Solids **355**, 1853 (2009).
[13]R. Demoulin, G. Beainy, C. Castro, P. Pareige, L. Khomenkova, C. Labbé, F. Gourbilleau, and E. Talbot, Nano Futures **2**, 035005 (2018).
[14]V. Monteseguro *et al.*, Opt. Mater. Express **5**, 1661 (2015).
[15]C. Stoneman and L. Esterowitz, Opt. Lett. **15**, 486 (1990).
[16]L. Feng, J. Wang, Q. Tang, L. F. Liang, H. B. Liang, and Q. Su, J. Lumin. **124**, 187 (2007).
[17]N. D. Afify, R. Grisenti, G. Dalba, C. Armellini, M. Ferrari, S. Larchelli, F. Rocca, and A. Kuzmin, Opt. Mater. **28**, 864 (2006).
[18]L. Miotti *et al.*, Appl. Phys. Lett. **85**, 4460 (2004).
[19]B. D. Cullity, *Elements of X-ray Diffractions* (Addison-Wesley, Reading, MA, 1972), p. 102.
[20]L. Khomenkova, Y.-T. An, C. Labbé, X. Portier, and F. Gourbilleau, ECS Trans. **45**, 119 (2012).
[21]T. V. Torchynska, Y. Goldstein, A. Many, J. Jedrzejewskii, and A. V. Kolobov, Microelectron. Eng. **66**, 83 (2003).
[22]L. Khomenkova *et al.*, J. Lumin. **102–103**, 705 (2003).
[23]O. Jambois, F. Gourbilleau, A. J. Kenyon, J. Montserrat, R. Rizk, and B. Garrido, Opt. Express **18**, 2230 (2010).
[24]B. Garrido, C. García, S.-Y. Seo, P. Pellegrino, D. Navarro-Urrios, N. Daldosso, L. Pavesi, F. Gourbilleau, and R. Rizk, Phys. Rev. B **76**, 245308 (2007).
[25]M. Wojdak, M. Klik, M. Forcales, O. B. Gusev, T. Gregorkiewicz, D. Pacifici, G. Franzò, F. Priolo, and F. Iacona, Phys. Rev. B **69**, 233315 (2004).
[26]S. Cueff, C. Labbé, J. Cardin, J.-L. Doualan, L. Khomenkova, K. Hijazi, O. Jambois, B. Garrido, and R. Rizk, J. Appl. Phys. **108**, 064302 (2010).
[27]A. Podhorodecki, J. Misiewicz, F. Gourbilleau, J. Cardin, and C. Dufour, Electrochem. Solid-State Lett. **13**, K26 (2010).
[28]J. Miniscalco, J. Lightwave Technol. **9**, 234 (1991).
[29]H. Song and Y. J. Kim, J. Eur. Ceram. Soc. **27**, 3745 (2007).
[30]X. T. Zhang, Y. C. Liu, J. G. Ma, Y. M. Lu, D. Z. Shen, W. Xu, G. Z. Zhong, and X. W. Fan, Thin Solid Films **413**, 257 (2002).
[31]H. J. Lozykowski, W. M. Jadwisienczak, and I. Brown, Appl. Phys. Lett. **74**, 1129 (1999).
[32]J. Silver, M. I. Martinez-Rubio, T. G. Ireland, G. R. Fern, and R. Withnall, J. Phys. Chem. B **105**, 948 (2001).
[33]XPS database, see https://srdata.nist.gov/xps/selEnergyType.aspx.